

Classification of Pathology in Diabetic Eye Disease

H. F. Jelinek¹, J. Leandro², R. M. Cesar, Jr² and M. J. Cree³

¹School of Community Health
Charles Sturt University, Albury, Australia

²Department of Computer Science
University of Sao Paulo, Brazil

³Dept. Physics and Electronic Engineering
University of Waikato, Hamilton, New Zealand

E-mail: HJelinek@csu.edu.au

Abstract

Proliferative diabetic retinopathy is a complication of diabetes that can eventually lead to blindness. Early identification of this complication reduces the risk of blindness by initiating timely treatment. We report the utility of pattern analysis tools linked with a simple linear discriminant analysis that not only identifies new vessel growth in the retinal fundus but also localises the area of pathology. Ten fluorescein images were analysed using seven feature descriptors including area, perimeter, circularity, curvature, entropy, wavelet second moment and the correlation dimension. Our results indicate that traditional features such as area or perimeter measures of neovascularisation associated with proliferative retinopathy were not sensitive enough to detect early proliferative retinopathy ($SNR = 0.76, 0.75$ respectively). The wavelet second moment provided the best discrimination with a SNR of 1.17. Combining second moment, curvature and global correlation dimension provided a 100% discrimination ($SNR = \infty$).

1 Introduction

In proliferative retinopathy new blood vessels are formed in the retina and emerge from the area of the optic disc and spread towards the macula or emerge from peripheral vessels [16]. Current prevalence of vision impairment due to retinopathy may be as high as 36% in the diabetic community. Timely intervention for diabetic retinopathy lessens the possibility of blindness [14, 18]. Any person with diabetes should expect to undergo ophthalmic examination at least annually. Initial screening and follow up assessment of the retinal fundus of diabetics is carried out by ophthalmologists, which is both expensive and time consuming when

large numbers of patients are examined [2, 19]. In addition barriers to screening in rural and remote areas exist and include distance required to travel, cost of screening and cultural reasons that often lead to indigenous people remaining in their communities rather than seeking health advice in larger urban centres. With advances in digital imaging and the development of computerised grading systems, automated reading and assessment of complications associated with the retinal fundus is becoming more sought after, especially in rural and remote areas.

Ophthalmologists have an 80 to 95% success rate in identifying proliferative retinopathy. This success rate decreases with eye obstruction such as cataract and for identifying earlier stages of proliferation without additional medical history [22]. However non-specialists perform no better than chance (50%). The National Health and Medical Research Council recommend that generally any screening procedure for identifying diabetic retinopathy needs to have a minimum sensitivity of 60% to maximise treatment outcomes and cost-effectiveness [21]. We concentrate on providing an automated procedure to assist in the identification of neovascularisation that meet NHMRC requirements, especially for rural health professionals. Automated reporting of neovascularisation involves the segmentation of the blood vessels from background in the digital image and provides an index of the stage of proliferation.

1.1 Mathematical assessment of optic fundus blood vessels

Research into automated processing of retinal fundus images has mainly concentrated on the identification of microaneurysms associated with preproliferative diabetic retinopathy [9, 15]. Mathematical techniques such as fractal analysis have been used in classification tasks as they

are able to quantify complex branching patterns including blood vessels [8, 17, 12]. Using an automated method that can detect neovascularisation with a minimum sensitivity of 60% is therefore an useful advancement as it would lessen the burden on ophthalmologists during initial population screening. The continuous wavelet transform (CWT) is a powerful and versatile tool that has been applied in many different image processing problems, including shape analysis [11].

2 Methods

2.1 Image Acquisition

Ten fluorescein angiographic retinal images (1024×1024 pixel) were obtained using a Topcon camera linked with Image 2000 software. These images were exported as TIFF images for manual tracing of the retinal vessels using the Object-Image imaging software (<http://rsb.info.nih.gov/nih-image/>) and analysed. Of the ten images five are control images (no disease present) and five are of neovascularisation (the diseased state). See Figure 1 for examples.

2.2 Morphological Feature Extraction

A number of features were measured on the vessel shapes. These included the area a , perimeter p , circularity ($c = p^2/a$) and wavelet fractal inspired measurements. These are described in the following.

2.3 Wavelet Transform Features

The wavelet transform is a mathematical tool that has been used in morphological studies of both 1D and 2D data. Instead of the 1D contour based approach of Cesar & Costa [6], we utilise the 2D approach [3]. The continuous wavelet transform (CWT) $T_\psi(\mathbf{b}, \theta, a)(\mathbf{x})$ of a retinal fundus image $f(\mathbf{x})$, with $\mathbf{x} = (x, y)$ is defined as:

$$T_\psi(\mathbf{b}, \theta, a)(\mathbf{x}) = C_\psi^{-\frac{1}{2}} \frac{1}{a} \int \psi^* (a^{-1} r_{-\theta}(\mathbf{x} - \mathbf{b})) f(\mathbf{x}) d^2x \quad (1)$$

where C_ψ , ψ , \mathbf{b} , θ and a denote the normalising constant, analysing wavelet, the displacement vector, the rotation angle and the dilation parameter respectively, with the asterisk denoting complex conjugation, and the partial form of the wavelet transform being the position representation [1]. The scale and angle parameters (a and θ respectively) were kept fixed for some *a priori* defined values $a = a_0$ and $\theta = \theta_0$. For the analysing wavelets used in this research we employed the first derivative of the Gaussian function [3]. Therefore, we define two analysing wavelets, $\psi_1(\mathbf{x})$ and

$\psi_2(\mathbf{x})$ as partial derivatives of the Gaussian, viz

$$\psi_1(\mathbf{x}) = \frac{\partial g(\mathbf{x})}{\partial x} \quad \text{and} \quad \psi_2(\mathbf{x}) = \frac{\partial g(\mathbf{x})}{\partial y} \quad (2)$$

where $g(\mathbf{x})$ denotes the 2D Gaussian. By using ψ_1 and ψ_2 as wavelets and the wavelet transform definition in Equation 1, we calculated the gradient wavelet as

$$\mathbf{T}_\psi[f](\mathbf{b}, a) = \begin{pmatrix} T_{\psi_1}[f](\mathbf{b}, a) \\ T_{\psi_2}[f](\mathbf{b}, a) \end{pmatrix} \quad (3)$$

Here, the wavelet transform \mathbf{T}_ψ for each pair (\mathbf{b}, a) is actually a vector whose components are the respective coefficients of the wavelet transform using ψ_1 and ψ_2 as the analysing wavelets. The wavelet gradient is calculated for every pixel in the image.

From the gradient waveform, \mathbf{T}_ψ , we obtain three complementary shape features to characterise the retinal fundus blood vessel pattern, namely the second wavelet moment, 2D curvature and entropy of orientation, calculated only on the pixels located at the boundary of the vessels.

2.4 Second Wavelet Moment

In order to characterise shape complexity we have utilised the modulus of \mathbf{T}_ψ , i.e.,

$$M_\psi[f](\mathbf{b}, a) = |\mathbf{T}_\psi| = \sqrt{(T_{\psi_1})^2 + (T_{\psi_2})^2} \quad (4)$$

providing a histogram that was calculated from the modulus of the wavelet transform M_ψ , for a fixed scale value of a [5]. Taking the frequency count of the i th bin of the histogram as p_i , we define the statistical moment of order q of M_ψ as a shape complexity measure, given by

$$m_q^M = \sum_i i^q p_i \quad (5)$$

and adopted the second moment, namely $q = 2$. The wavelet calculates the gradient vector at a given pixel by looking at a neighbourhood around the pixel.

2.5 Entropy of the Orientation

From \mathbf{T}_ψ and M_ψ the respective orientation of each gradient vector may be easily calculated as the angle associated to each vector and a histogram of gradient versus orientation. In order to quantify this dispersion, we have adopted the entropy s of the orientation distribution,

$$s = - \sum_i p_i \ln p_i \quad (6)$$

where the i now indicate histogram binning with respect to orientation θ .

2.6 2D Curvature

A measure of how the gradient vectors vary locally is obtained from the wavelet transforms that compose the gradient vectors, defined as the 2D curvature. The 2D curvature is defined as:

$$k = \nabla \cdot \frac{\nabla f}{\|\nabla f\|} = \frac{f_{xx}f_y^2 - 2f_xf_yf_{xy} + f_{yy}f_x^2}{(f_x^2 + f_y^2)^{3/2}} \quad (7)$$

where f_x , f_y , f_{xx} , f_{yy} and f_{xy} denote the first partial derivatives of f with respect to x and to y , and the second partial derivatives of f also with respect to x and y . These partial derivatives are estimated using the 2D wavelet transform in the same spirit described above for the gradients

2.7 Correlation Dimension

We utilised the correlation dimension as a complexity measure as previously discussed in the literature [13]. The correlation dimension is defined by

$$D_2 = \lim_{\epsilon \rightarrow 0} \frac{\log_{10} C(\epsilon)}{\log_{10} \epsilon} \quad (8)$$

where $C(\epsilon)$ is the correlation integral calculated with an analysing disc of diameter ϵ . This procedure leads to a graph $C(\epsilon)$ versus ϵ from which a log-log plot-based line fitting is able to estimate the correlation dimension. The linear portion of the log-log slope is determined by two methods. The median correlation dimension is determined by measuring the slope for short segments within the log-log plot and taking the median value of all determined slopes. The global correlation dimension is determined by taking the wavelet transform of the log-log plot using the third derivative of the Gaussian as mother wavelet [7] to establish the end points of the linear region, and calculating the slope from the two end points.

2.8 Statistical Analysis

Basic statistical information, including mean and standard deviation, was calculated on the individual classes (control and neovascularisation) for each of the measured features. Assuming a Gaussian distribution for the underlying probability distribution for each feature measured over each class, we arrived at SNR values, which give an indication of the predictive power, for each individual feature.

To analyse the data for predictive power of the combined features for classification, linear discriminant analysis (LDA) was performed on the matrix representing the data of the images. Features were normalised so that each feature has zero mean and unit standard deviation. LDA

was performed with training and testing with the complete dataset, and with cross-validation by testing on each of the individual images with the classifier trained on the other nine images.

A forward feature selection process using LDA as the classifier was also tried to select the best features. For this we varied the constant term of the LDA discriminant function to bias the discriminant towards one class and then the other class, thus obtaining a series of sensitivity and specificity values for detecting the diseased state (neovascularisation). A receiver operating curve (ROC) was fitted to the specificity and sensitivity values according to the model described by Metz [20], and the area under the curve (AUC), which can be shown to be a monotonically increasing function of the SNR under certain not too restrictive assumptions [4], was used to test the efficacy of the classifier. At each stage the one best feature out of the remaining features was added to the subset of features currently selected and this process was continued until all features were added or no feature improved the classification.

3 Results

Table 1 provides the basic statistical results for each of the features analysed on the ten images. On the naïve assumption of underlying Gaussian probability distributions for each of the classes of each feature the second moment comes out as the best single feature with a SNR of 1.17.



Figure 1. Fluorescein angiographic retinal images of a control patient (left) and with neovascularisation (right)

Figure 1 shows a fluorescein angiographic retinal image of a control and a neovascular retinal fundus. Figure 2 shows for the same images used in Figure 1 the wavelet gradient modulus used in the calculation of the second moment and curvature as 2D output that allows localisation of pathology.

Using LDA as a classifier, trained and tested on the full feature data set, perfect classification was achieved. This result should be treated with scepticism as the discriminant function involved the cancellation of the area, perimeter and circularity terms with each other, then multiplying that re-

Table 1. Statistical properties of the individual classes for the measured features.

Feature	Control Mean \pm SD	Neovascularisation Mean \pm SD	Discriminative Power (SNR)
Area	85000 ± 16000	100000 ± 23000	0.76
Perimeter	33200 ± 6200	39000 ± 8900	0.75
Circularity	$(13.0 \pm 2.4) \times 10^6$	$(15.1 \pm 3.5) \times 10^6$	0.73
2nd moment	4073 ± 19	4100 ± 25	1.17
Entropy	5.57 ± 0.01	5.58 ± 0.02	0.54
Curvature	290.2 ± 4.2	295.0 ± 5.2	1.02
CD ¹ median	1.63 ± 0.08	1.62 ± 0.09	0.05
CD global	1.56 ± 0.04	1.58 ± 0.06	0.54

¹ CD = correlation dimension.

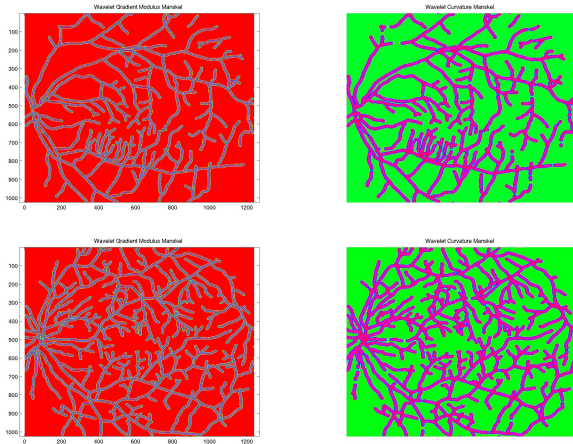


Figure 2. Colour coded image of wavelet gradient modulus (left) and curvature (right) of the control (top) and neovascular (bottom)

sult by five orders of magnitude above the remaining terms. This is the result of training on too few data.

Running the forward selection on the feature data set with LDA as the classifier identified three features, namely circularity, second moment and global correlation dimension, as all that is needed for perfect classification where the classification is both trained and tested on the full data set.

We also examined the utility of a cross-validation on the LDA where the classifier is trained with nine images and tested on the one not included in training. This is repeated for leaving each image in turn out of the training. The results of the cross-validation on the manual dataset (using all features) indicated that all neovascularisation images were correctly classified but two of the control images were not. Interestingly perfect classification is obtained by excluding the 'area' and 'perimeter' features. The removal of these features, which are highly correlated to each other and to

circularity, has improved the classification.

4 Discussion

Diabetes and its associated complications, including proliferative diabetic retinopathy, has been identified as a significant growing global public health problem. Direct screening programmes such as those based on visits to the ophthalmologist for retinal fundus assessment currently fail to screen between 15 and 62% of patients each year [10]. A large proportion of these people develop potentially sight threatening eye disease, which even at an advanced stage may not cause any symptoms, yet treatment with a laser can prevent visual loss in up to 98% of people if detected early enough [18]. An important step towards reducing the numbers of individuals seriously affected by diabetic retinopathy is to simplify the procedure used to identify the condition and ensure that early eye examinations become routine for all people with diabetes.

Traditional features such as area, perimeter and fractal dimension are not sensitive enough to discriminate between the control retinal fundi and retinal fundi displaying neovascularisation. Our feature analysis suggests that either the second wavelet moment alone or in combination with the curvature and global correlation dimension add to the accuracy of the classification.

This present study is limited in two ways. First, manually obtained vessel segmentations were used for analysis. Ideally the whole process should be automated and studies are currently being undertaken to develop an automated means of segmenting the blood vessels [7]. Second, the number of images used in this study are few, hence a question remains whether the images used truly incorporate the amount of variation present in a large population of retinal images. For this reason we only used LDA for classification. It is planned to repeat the study, with automated vessel segmentation, on a larger corpus of retinal images, and with more powerful classification algorithms.

Acknowledgements: HJ was funded for this project by

Charles Sturt University and the Australian Diabetes Association. RMC is grateful to FAPESP (99/12765-2) and to CNPq (300722/98-2, 468413/00-6)

References

- [1] J. P. Antoine, P. Carette, R. Murenzi, and B. Piette. Image analysis with two-dimensional wavelet transform. *Sig. Proc.*, 31:241–272, 1993.
- [2] R. Ariysau, P. Lee, K. Linton, L. L. Bree, S. Azen, and A. Siu. Sensitivity, specificity and predictive values of screening tests for eye conditions in a clinic-based population. *Ophthalmol.*, 103:1751–1760, 1996.
- [3] A. Arnéodo, N. Decoster, and S. G. Roux. A wavelet-based method for multifractal image analysis: I. Methodology and test applications on isotropic and anisotropic random rough surfaces. *Eur. Phys. J. B*, 15:567–600, 2000.
- [4] H. H. Barrett, C. K. Abbey, and E. Clarkson. Objective assessment of image quality. III. ROC metrics, ideal observers and likelihood-generating functions. *J. Opt. Soc. Am. A*, 15:1520–1535, 1998.
- [5] O. M. Bruno, R. M. Cesar, Jr, L. A. Consularo, and L. da F. Costa. Automatic feature selection for biological shape classification in SYNERGOS. In *Proceedings of the Brazilian Conference on Computer Graphics, Image Processing and Vision (SIBGRAPI)*, pages 363–370, Rio de Janeiro, Brazil, 1998.
- [6] R. M. Cesar, Jr and L. da F. Costa. Neural cell classification by wavelets and multiscale curvature. *Biol. Cybernet.*, 79:347–360, 1998.
- [7] R. M. Cesar, Jr and H. F. Jelinek. Segmentation of retinal fundus vasculature in nonmydriatic camera images using wavelets. In J. S. Suri and S. Laxminarayan, editors, *Angiography and Plaque Imaging*, pages 193–224. CRC, Boca Raton, Fl., 2003.
- [8] D. Cornforth, H. F. Jelinek, and L. Peichl. Fractop: A tool for automated biological image classification. In *Proceedings of the Sixth AI Australasia-Japan Workshop*, pages 141–148, Canberra, Australia, 2002.
- [9] M. J. Cree, J. A. Olson, K. C. McHardy, P. F. Sharp, and J. V. Forrester. A fully automated comparative microaneurysm digital detection system. *Eye*, 11:622–628, 1997.
- [10] M. Cummings. Screening for diabetic retinopathy. *Prac. Diab. Int.*, 19(1):5, 2002.
- [11] L. da F. Costa and R. M. Cesar, Jr. *Shape Analysis and Classification: Theory and Practice*. CRC Press, Boca Raton, FL, 2001.
- [12] A. Daxer. The fractal geometry of proliferative diabetic retinopathy: Implications for the diagnosis and the process of retinal vasculogenesis. *Curr. Eye Res.*, 12:1103–1109, 1993.
- [13] F. Family, B. R. Masters, and D. E. Platt. Fractal pattern formation in human retinal vessels. *Physica D*, 38:98–103, 1989.
- [14] U. Freudentsein and J. Verne. A national screening programme for diabetic retinopathy. *Br. Med. J.*, 323:4–5, 2001.
- [15] J. H. Hipwell, F. Strachan, J. A. Olson, K. C. McHardy, P. F. Sharp, and J. V. Forrester. Automated detection of microaneurysms in digital red-free photographs: a diabetic retinopathy screening tool. *Diabetic Medicine*, 17:588–594, 2000.
- [16] J. Kanski. *Clinical Ophthalmology: A Systematic Approach*. Butterworth-Heinemann, London, 1989.
- [17] G. Landini. Applications of fractal geometry in pathology. In P. M. Iannaccone and M. Khokha, editors, *Fractal Geometry in Biological Systems*, pages 205–245. CRC, Amsterdam, Netherlands, 1996.
- [18] S. J. Lee, C. Sicari, C. A. Harper, H. R. Taylor, and J. E. Keefe. Program for the early detection of diabetic retinopathy: A two year follow-up. *Clin. Exp. Ophthalmol.*, 29:12–25, 2001.
- [19] V. Lee, R. Kingsley, and E. Lee. The diagnosis of diabetic retinopathy: Ophthalmology versus fundus photography. *Ophthalmol.*, 100:1504–1512, 1993.
- [20] C. E. Metz. ROC methodology in radiologic imaging. *Invest. Radiol.*, 21:720–733, 1986.
- [21] National Health and Medical Research Council. *Management of Diabetic Retinopathy Clinical Practice Guidelines*. Australian Government, Canberra, 1997.
- [22] E. Sussman, W. Tsiaris, and K. Soper. Diagnosis of diabetic eye disease. *J. Am. Med. Assoc.*, 247:3231–3234, 1982.